The molecular basis for protein kinase A anchoring revealed by solution NMR

Marceen Glavic Newlon[1], Melinda Roy[1], Dimitrios Morikis[1], Zachary E. Hausken[2], Vincent Coghlan[3], John D. Scott[2] and Patricia A. Jennings[1]

[1]Department of Chemistry and Biochemistry, University of California, San Diego, La Jolla, California 92093-0359. [2]Howard Hughes Medical Institute, Vollum Institute, Portland, Oregon 97201-3098. [3]R.S. Dow Neurological Sciences Institute, Oregon Health Sciences University, Portland, Oregon 97209-1595.

Compartmentalization of signal transduction enzymes into signaling complexes is an important mechanism to ensure the specificity of intracellular events. Formation of these complexes is mediated by specialized protein motifs that participate in protein–protein interactions. The adenosine 3′,5′-cyclic monophosphate (cAMP)-dependent protein kinase (PKA) is localized through interaction of the regulatory (R) subunit dimer with A-kinase-anchoring proteins (AKAPs). We now report the solution structure of the type II PKA R-subunit fragment RIIα(1–44), which encompasses both the AKAP-binding and dimerization interfaces. This structure incorporates an X-type four-helix bundle dimerization motif with an extended hydrophobic face that is necessary for high-affinity AKAP binding. NMR data on the complex between RIIα(1–44) and an AKAP fragment reveals extensive contacts between the two proteins. Interestingly, this same dimerization motif is present in other signaling molecules, the S100 family. Therefore, the X-type four-helix bundle may represent a conserved fold for protein–protein interactions in signal transduction.

Many intracellular signal transduction pathways utilize second messengers such as calcium, phospholipids or cAMP to exert their effects within cells. They typically do so by the selective activation and repression of two enzyme groups: protein kinases that catalyze the phosphorylation of specific protein substrates and protein phosphatases that catalyze the dephosphorylation reaction[1]. Multiple regulatory mechanisms exist to restrict the spatial and temporal resolution of kinase and phosphatase activity. In this way, the appropriate substrate proteins become phosphorylated at the right place and time in the cell to favor signaling specificity[1–3]. Anchoring proteins have been identified that direct individual kinases or phosphatases to defined intracellular compartments. Furthermore, multivalent anchoring proteins have been described that form localized signaling scaffolds which respond to distinct activation signals[1–5]. Accordingly, enzyme compartmentalization has emerged as a principle mechanism to ensure the precision and fidelity of signal transduction events.

Compartmentalization of the PKA holoenzyme is mediated through association of the R subunits with AKAPs[5–7]. Structure–function analyses have demonstrated that R-subunit dimerization, maintained by the first 44 residues (Fig. 1*a*), is a prerequisite for AKAP binding and that side chains in this region are determinants for anchoring interactions[6–8]. While the crystal structures for the catalytic C subunit[9] and a monomeric frag-

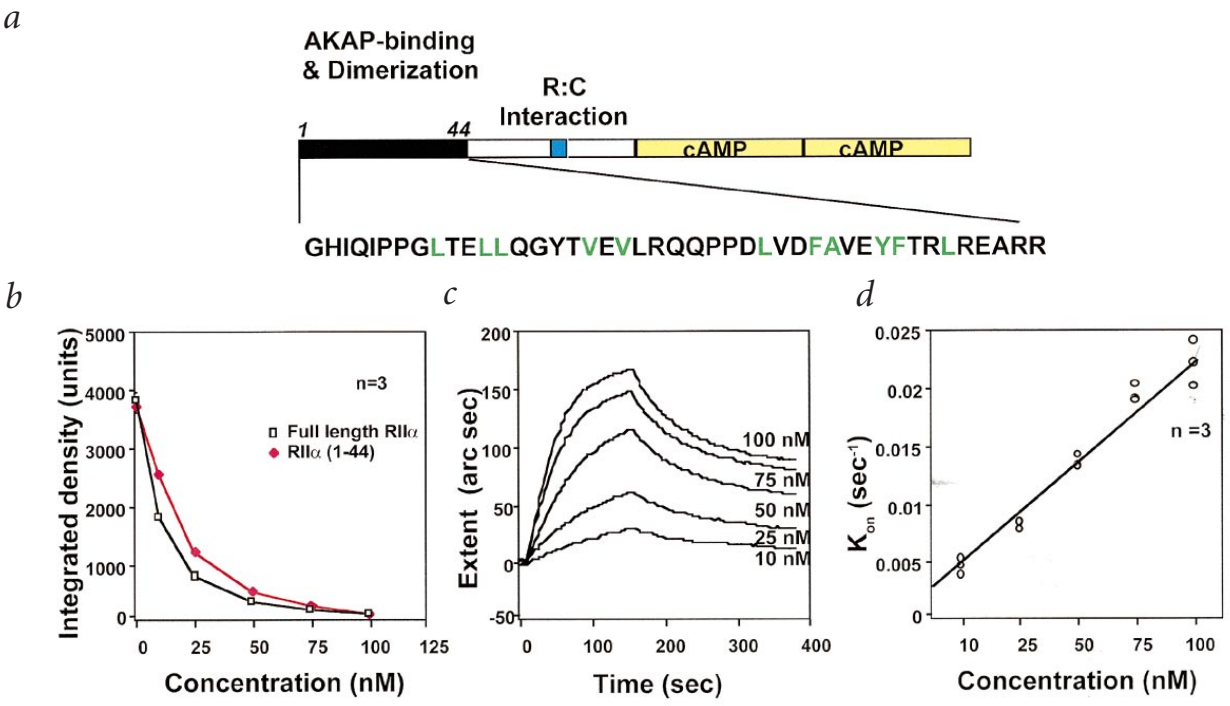

Fig. 1 Characterization of the RIIα(1–44) fragment. ***a***, Schematic representation of the domain structure of RIIα. The AKAP-binding/dimerization domain lies at the extreme N-terminus followed by the R:C pseudosubstrate site in blue and the two cAMP-binding domains in yellow. The amino acid sequence for residues 1–44 is indicated in single-letter amino acid code. Residues highlighted in green indicate conserved hydrophobic residues in all R isoforms. ***b***, RII competition overlays using increasing concentrations of full-length protein (□) or RIIα(1–44) (◆) as the competitors, as detected by surface plasmon resonance. ***c***, Real-time binding events to immobilized Ht31(493–515) are depicted at defined concentrations of RIIα(1–44). Binding was measured as a function of plasmon resonance extent (arc sec) ***d***, Measured on rates (s^{-1}) were plotted against concentration of RIIα(1–44). All measurements were done in triplicate.

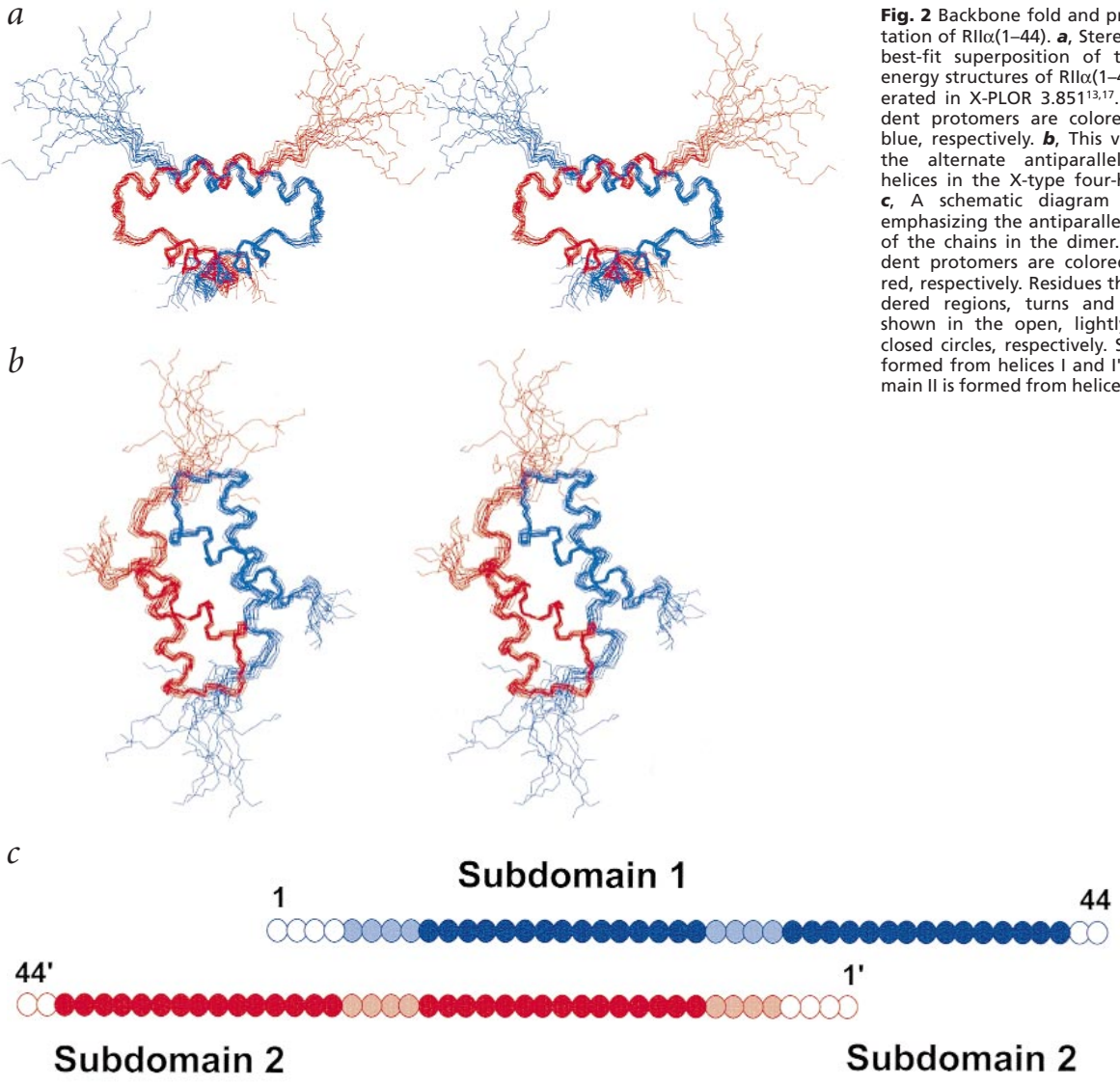

Fig. 2 Backbone fold and protomer orientation of RIIα(1–44). ***a***, Stereo views of the best-fit superposition of the 17 lowest energy structures of RIIα(1–44) dimer generated in X-PLOR 3.851[13,17]. The independent protomers are colored in red and blue, respectively. ***b***, This view highlights the alternate antiparallel packing of helices in the X-type four-helix bundle[19]. ***c***, A schematic diagram of RIIα(1–44) emphasizing the antiparallel arrangement of the chains in the dimer. The independent protomers are colored in blue and red, respectively. Residues that form disordered regions, turns and α-helices are shown in the open, lightly shaded and closed circles, respectively. Subdomain I is formed from helices I and I', while subdomain II is formed from helices II and II'.

ment of the type I R-subunit cAMP-binding domains[10] have been resolved, there is no detailed structural information on the RII–AKAP interaction. We reasoned that a recombinant fragment of RIIα, called RIIα(1–44), was an appropriate candidate for structural determination. This fragment and full-length RIIα exhibit similar AKAP-binding affinity for the human thyroid anchoring peptide, Ht31(493–515), as assessed in a semiquantitative, solid-phase competition assay (Fig 1*b*). The dissociation constant for the Ht31(493–515)–RIIα(1–44) interaction was 16 ± 1 nM (n = 3), as measured by surface plasmon resonance (Fig. 1*c,d*), similar to the value measured for full-length RIIα[11].

RIIα(1–44) Structure

We employed triple-resonance, three-dimensional nuclear magnetic resonance (NMR) techniques to determine the solution structure of the RIIα(1–44) fragment. The sample pH of 4.0 was necessary to avoid nonspecific protein aggregation. The dimeric structure of RIIα(1–44) and high-affinity interactions with AKAPs are maintained at this pH[12]. A single set of backbone H^N correlation signals for the 44-residue protomer is observed in the NMR spectra, indicating that the protein is a symmetric dimer in solution. As the majority of long-range nuclear Overhauser effect (NOE) resonances arise from side chain–side chain interactions, ^{13}C-edited experiments were especially useful in obtaining the necessary data for structure calculations. However, derivation of distance restraints for the solution structure of a homodimer is complicated by the fact that both intermolecular and intramolecular contacts give rise to NOEs. Thus discriminating between the two types of NOEs becomes of utmost importance[13]. Critical intermolecular NOEs were assigned unambiguously through comparison of 3D ^{13}C-edited[14] and ^{13}C-edited (ω_2)–^{12}C-filtered (ω_1) / ^{13}C-filtered (ω_3) NOESY[15] data. In addition, homonuclear NOESY experiments[16] helped in the identification of a subset of intermonomer aliphatic–aromatic interactions because several observed NOEs were inconsistent with the expected results for intramolecular contacts in regions with regular helical structure. In all, 76 (38 per monomer) intermolecular contacts were assigned.

A total of 505 distance, 25 backbone dihedral and 19 hydrogen bond restraints (per monomer) were used to generate an ensemble of 17 structures with the program X-PLOR 3.851 (Fig. 2*a,b*)[13,17]. Structural statistics (Table 1*a*) and stereo views of the

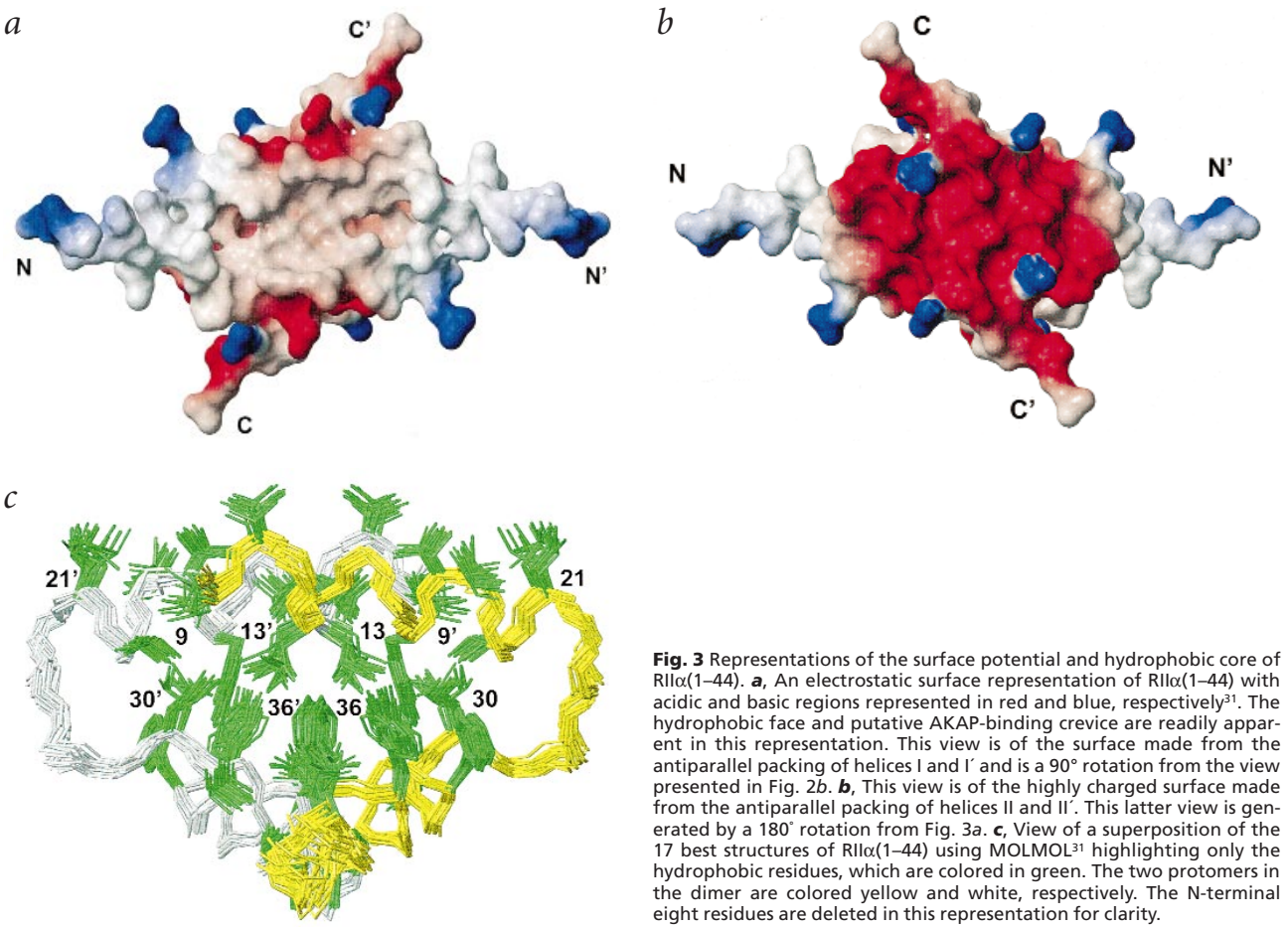

Fig. 3 Representations of the surface potential and hydrophobic core of RIIα(1–44). ***a***, An electrostatic surface representation of RIIα(1–44) with acidic and basic regions represented in red and blue, respectively[31]. The hydrophobic face and putative AKAP-binding crevice are readily apparent in this representation. This view is of the surface made from the antiparallel packing of helices I and I′ and is a 90° rotation from the view presented in Fig. 2*b*. ***b***, This view is of the highly charged surface made from the antiparallel packing of helices II and II′. This latter view is generated by a 180° rotation from Fig. 3*a*. ***c***, View of a superposition of the 17 best structures of RIIα(1–44) using MOLMOL[31] highlighting only the hydrophobic residues, which are colored in green. The two protomers in the dimer are colored yellow and white, respectively. The N-terminal eight residues are deleted in this representation for clarity.

best-fit superposition of these structures in two orientations (Fig. 2*a,b*) demonstrate that the structures are well defined and in excellent agreement with the NMR data, with no NOE violation >0.4 Å, no dihedral-angle violation >5° and good covalent geometry. The precision of the solution structure was determined from a comparison of the mean structure with the individual structures and expressed as the average root-mean-square deviation (r.m.s.d.; Table 1*a*). The best structure contained 0 bad contacts per 100 residues.

The structure of each protomer begins with an extended region at the N-terminus followed by a turn into a helix-turn-helix motif (Fig. 2*a,b*). The structure can be subdivided into two functional regions: the first 23 residues form the AKAP-binding surface and residues 24–44 encompass the bulk of the dimer contacts (Fig 2*c*). Helices I and II in the monomer are nearly orthogonal to one another with an interhelical angle of 125° (Table 1*b*). Several strong intermolecular NOE crosspeaks, including interactions between Leu 21 and Ile 5, Leu 21 and Pro 6, Ala 32 and Phe 36, and Asp 30 and Arg 40, orient the monomers in an antiparallel arrangement. Therefore, the RII dimer adopts a similar topology to RI (antiparallel)[8] and opposite to that proposed for the type I- guanosine 3',5'-cyclic monophosphate (cGMP)-dependent protein kinase (parallel)[18]. Additional NOEs confirm that the monomers pack in an X-type four-helix bundle with an alternating pattern of antiparallel and orthogonal helix–helix interactions around the bundle (Fig. 2)[19]. With respect to Crick's structural hypothesis for optimal packing in helical proteins, the X-type four-helix bundle leaves many open knobs and holes[19,20]. Thus, this motif is commonly found in the interior of proteins where additional helices pack with this substructure to form a globular fold. In the absence of these additional tertiary interactions, as is the case with RIIα(1–44), this packing arrangement may invite specific protein–protein interactions such as RII–AKAP anchoring. A surface representation of RIIα(1–44) is consistent with this proposal (Fig. 3*a,b*).

The RIIα(1–44) dimer has extensive, well-ordered hydrophobic interactions in its core (Fig. 3*c*). Residues forming important dimer contacts include Ile 5, Pro 6, Leu 9, Leu 12, Leu 13, Tyr 16, Val 20 and Leu 21 in helix I, and Leu 28, Val 29, Ala 32, Val 33, Phe 36, Thr 37 and Leu 39 in helix II. These residues form an extended hydrophobic surface of the dimer interface. There is also a strong, solvent-accessible, intermolecular hydrogen bond between Asp 30 and Arg 40 (2.9 ± 0.6 Å separation). In total, 20% (1,600 Å^2) of the available surface area in the monomer is buried in the interface upon dimer formation. Sequence alignment of all R isoforms (RIα, RIβ, RIIα, RIIβ) reveals a conservation of this hydrophobic dimerization core (Fig. 1*a*)[8]. Deletion and mutagenesis experiments confirm that removal of residues 1–10 or alteration of residues Leu 13 or Phe 36 abolishes dimerization and AKAP interaction[7,21]. The conserved aromatic residue at position 16 in RIIα and RIIβ (α: Tyr; β: Phe) is not present in RI. Instead, the RI isoforms contain two disulfide bonds in the dimerization domain that are

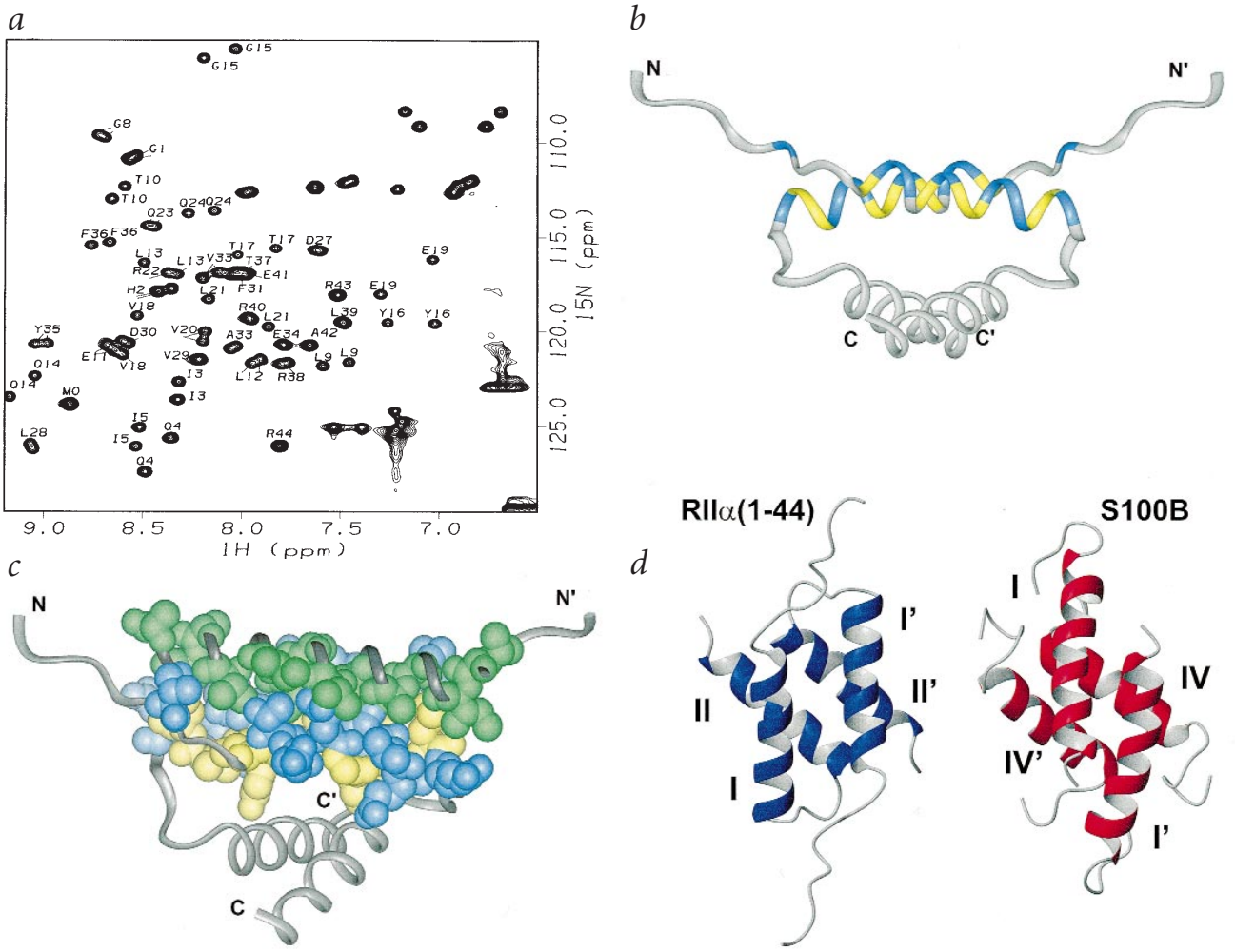

Fig. 4 Analysis of anchoring interactions. ***a***, The ^{1}H-^{15}N HSQC spectrum of the RIIα(1–44)–Ht31(493–515) complex at 25 °C, pH 4.0. All backbone amide resonances are identified. Crosspeaks due to side chains are not labeled. ***b***, Summary of the chemical-shift changes observed for RIIα(1–44). Regions undergoing significant chemical-shift perturbation are mapped onto a ribbon diagram of RIIα(1–44). The presented structure is in the same orientation as in Fig. 2*a*. The yellow and blue regions indicate residues that undergo chemical-shift changes >0.1 and 0.2 p.p.m., respectively. ***c***, A model of the RIIα(1–44)–Ht31(493–515) complex. This view is presented in the same orientation as in Fig. 2*a*. The side chains of residues of RIIα(1–44) highlighted in (*b*) are represented with their van der Waals radii and are colored in yellow and blue as in (*b*). The Ht31(493–515) backbone is shown in dark gray, and the hydrophobic side chains are shown in green. All other side chains in the complex are deleted for clarity. ***d***, A comparison of the dimerization interfaces of RIIα(1–44) and S100B using MOLMOL[31]. The ribbon representation of RIIα(1–44) is presented in the same orientation as in Fig. 2*b*. Helices I and I′ in RIIα(1–44) form the bulk of the AKAP interaction sites, while only part of helices IV and IV′ in S100B interact with target peptides[25,27].

absent in RII but confer increased stability to this domain when oxidized[22]. This property may provide an added measure of specificity by preventing the formation of RI–RII heterodimers *in vivo*.

AKAP binding surface

In addition to the extensive hydrophobic core, the protein presents an extended, solvent-accessible hydrophobic surface (Fig. 3*a,c*). This surface is formed by the antiparallel array of helices I and I′. Residues Ile 5, Pro 6, Thr 10, Thr 17, Val 18 and Leu 21 are strictly conserved in the type II protein and afford a recognition surface for interactions with AKAPs, supporting previous mutagenesis studies that affect AKAP interaction[7,21]. In addition His 2, Glu 11 and Arg 22 may provide a means of gaining specificity in the AKAP–RII interaction through ionic interactions. Indeed, all anchoring peptides identified thus far have, in addition to conserved hydrophobic residues, a positively charged central residue and at least one negatively charged terminal residue that could complement the charges on the surface of RII (Fig. 3*a,b*)[4,6].

To evaluate the proposal that this surface is involved in AKAP interactions, a series of ^{1}H-^{15}N heteronuclear single-quantum coherence (HSQC) spectra[23] were acquired on samples containing ^{15}N-labeled RIIα(1–44) and varying concentrations of the AKAP inhibitor peptide, Ht31(493–515). Ht31(493–515) binds to RIIα(1–44) with a stoichiometry of one per RIIα dimer and with nanomolar affinity (Fig. 1*b,c*)[4,6]. Since Ht31(493–515) is not palindromic, it induces chemical-shift splitting as well as chemical-shift changes upon binding to the symmetric dimer. The ^{1}H-^{15}N HSQC spectrum of the 1:1 complex is given in Fig. 4*a*. Amide proton resonances that undergo chemical-shift changes upon complex formation have been identified (Fig. 4*a*)

Table 1 Structural statistics for the 17 lowest energy structures of RIIα(1–44) and comparison of the interhelical angles for X-type bundle dimeric proteins

a, NMR statistics			
NOE-derived restraints			
Type of restraint	Number of restraints		
Intraresidue (i - j = 0)	185		
Sequential (|i - j| = 1)	136		
Medium (1 < |i - j| ≤4)	95		
Long (|i - j| >4)	25		
Intermolecular	38		
Ambiguous	26		
Dihedral	25		
Hydrogen bond	19		
Total NOEs	505		
Number of NOEs per residue	11.0		
R.m.s.d. values[1]			
Residues	Relative to mean (backbone N,Cα,C′)	Relative to mean (heavy atoms)	
5–42, 5'–42'	0.63 ± 0.12	1.00 ± 0.08	
9–42, 9'–42'	0.55 ± 0.08	0.96 ± 0.055	
9–23[1]	0.30 ± 0.08	0.83 ± 0.65	
28–42[1]	0.35 ± 0.064	0.86 ± 0.57	
Energy statistics			
Energy (kcal mol^{-1})	RIIα(1–44) ensemble	RIIα(1–44) best[2]	
Total	205.9 ± 6.5	193.3	
Bond	12.1 ± 0.3	11.6	
Angle	112.5 ± 1.3	110.6	
Improper	14.6 ± 0.5	14.4	
Dihedral	0.00 ± 0	0.00	
Van der Waals	40.0 ± 1.4	38.0	
NCS	0.061 ± 0.019	0.052	
NOE	26.7 ± 4.5	18.6	
b, Interhelical angles			
Helices	RIIα(1–44)	S100B(ββ)	Calcyclin
I–I' (IV–IV')[3]	156	159	148
II–II' (I–I')[3]	151	155	144
I–II (IV–I)[3]	125	119	124

[1]R.m.s.d. values for residues 9–23 and 28–42 are reported per monomer.
[2]The best structure is defined as the structure with the smallest deviation from the mean. No 6–12 Lennard Jones, hydrogen bond or electrostatic energy terms were used to generate the structures.
[3]The helices in parentheses correspond to those involved in the dimer interface of S100B and calcyclin. The errors in the reported interhelical angles of RIIα(1–44) are ±5°.

and map to a well-defined surface on RIIα(1–44) (Fig. 4*b*). This region is identical to the AKAP-binding surface implicated by visual analysis of the electrostatic surface (Fig. 3*a*). The chemical-shift changes observed for residues Leu 9, Thr 10, Glu 11, Leu 13, Gln 15, Tyr 16, Thr 17, Val 18, Glu 19, Leu 21 and Arg 22 in RIIα(1–44) upon complex formation are likely due to direct helix–helix contacts between the two proteins, while those changes in residues 1–6 could reflect either structural changes in the N-terminus and/or sites of AKAP interaction.

Changes in chemical shift upon addition of Ht31(493–515) can result from either direct contacts or structural changes as both processes will alter the nuclear chemical environment. Chemical-shift changes observed for residues in helix I are likely due to direct helix–helix contacts rather than gross structural changes for the following reasons: (*i*) The largest chemical-shift changes map to a well-defined surface on RIIα(1–44) as expected for direct contact; (*ii*) ^{13}Cα chemical-shift analysis[24] of RIIα(1–44) indicates that the helical boundaries are identical in the apo and complex structures (data not shown); (*iii*) if the overall conformation of RIIα(1–44) changed significantly upon complex formation, the observed chemical-shift changes would be expected to be more widespread. However, chemical-shift changes observed for residues 1–6 in RIIα(1–44) are likely due to both binding and structural changes, as this region is disordered in the apo structure and most likely more ordered in the complex since residues in this region make important AKAP contacts. A model for the structure of the RIIα(1–44) domain–Ht31(493–515) complex where the hydrophobic side chains of residues Ile 3, Ile 5, Leu 9, Thr 10, Leu 13, Thr 17, Val 18 and Leu 21 on RIIα can make extensive hydrophobic interactions with residues on Ht31(493–515) is shown in Fig. 4*c*. Structure determination of the bound peptide is currently being investigated that requires both reassignment of the RIIα(1–44) spectrum and assignment of Ht31(494–515).

The structure of the RII domain and the model of the complex with the AKAP peptide reported herein confirms and significantly extends previously published biochemical data[7,21]. The hydrophobic surface of the RIIα(1–44) domain is the site of

direct AKAP interaction, requiring large hydrophobic residues in the AKAP for R-subunit binding[6]. Residues Ile 3 and Ile 5 in RII, important for AKAP binding[7], most likely form strong hydrophobic interactions by wrapping around the AKAP peptide. Our structure also explains why a Val 20–Leu 21 double mutation in RIIβ diminishes AKAP binding[21]. Leu 21 extends out along the Ht31-binding region of RII and likely interacts with the AKAP, whereas Val 20 is undoubtedly involved in maintaining a stable dimer (Fig. 3*c*).

The X-type four-helix bundle

The X-type four-helix bundle dimerization motif is present in another class of signaling molecules, the S100 proteins S100B[25,26] and calcyclin[27] (Table 1*b;* Fig. 4*d*). Interestingly, this same dimerization motif is involved in additional protein–protein interactions between S100B and p53 (ref. 25). In the latter case, the proteins only interact in the presence of Ca^{2+}, exposing the X-type bundle. The EF-hands in S100B supply additional helices involved in p53 binding[25]. While there are clear structural similarities between S100 and RII, there are notable differences. For example, two p53 molecules bind per S100 dimer, maintaining a symmetric complex, whereas only one AKAP binds per RII dimer, inducing asymmetry. Also there are distinct differences in binding affinities: p53 binds to S100B with micromolar affinity, whereas AKAPs bind RII 1,000-fold tighter, in the low nanomolar range. Thus, this X-type bundle structural fold is able to produce a variety of discrete interaction surfaces determined by the specific protein's sequence and quaternary structure. The dimeric X-type bundle found in RII and S100B may be a general motif involved in protein–protein interactions, providing a stable protein platform for the assembly of signaling complexes.

Methods

RIIα competition assays. Recombinant RIIα(1–44) was expressed and purified from *Escherichia coli*[12]. RII competition overlays were performed with ^{32}P-radiolabeled RIIα using increasing concentrations of full-length protein or RIIα(1–44) as the competitor[7]. Surface plasmon resonance measurements of the RIIα(1–44)–Ht31(493–515) interaction were performed as previously described[28].

NMR experiments. All NMR experiments were performed at 25 °C on either a Bruker DMX500 or DRX600 spectrometer using a triple-resonance gradient probe. RIIα(1–44) NMR sample preparation and assignment of backbone and side-chain nuclei have been described elsewhere[12]. Additional NOE experiments included a 100 ms 2D NOESY[16] and a 3D ^{13}C-edited HMQC–NOESY[14] (τ_m = 150 ms). $J_{NH\text{-}H\alpha}$ coupling constants were determined based on the intensity ratio of the crosspeak to the diagonal in the HNHA experiment[29]. Coupling constants >8 Hz were given φ restraints of -140° ± 40° and those <5 Hz were -60° ± 30°. All experiments were processed using Felix 95.0 software (Molecular Simulations, Inc.).

To distinguish between intramolecular and intermolecular NOEs, an asymmetrically labeled sample of one unlabeled protomer and one ^{13}C-^{15}N-labeled protomer was prepared. This was achieved by mixing equal volumes of 2 mM unlabeled RIIα(1–44) and 2 mM ^{13}C-^{15}N-labeled RIIα(1–44), and unfolding in 5 M guanidine hydrochloride. The unfolded samples were refolded by slow dilution into 20 mM sodium phosphate buffer, pH 4.0. The sample was concentrated by Centricon (Amicon, Inc.) to 1 mM asymmetrically labeled dimer. This sample was used to collect a 3D ^{13}C-edited (ω_2)–^{12}C-filtered (ω_1) / ^{13}C-filtered (ω_3) NOESY[15] with a 150 ms mixing time.

Structure calculations. Interproton distance restraints were obtained through measured peak volumes calibrated against known distances in elements of regular secondary structure. NOEs were classified as strong (1.8–2.7 Å), medium (1.8–3.3 Å), weak (1.8–5.0 Å) or very weak (1.8–6.0 Å). Dimer structures were calculated as described by Nilges[13]. In the initial rounds of structure calculations, NOEs were either classified as resulting from only intermolecular contacts [determined from the ^{13}C-edited (ω_2)–^{12}C-filtered (ω_1) / ^{13}C-filtered (ω_3) NOESY[14]] or as ambiguous (resulting from both intermolecular and intramolecular contacts). In the final rounds, NOEs were separated into three categories: intramolecular, intermolecular and ambiguous. In the final round of calculations, 49 final structures were generated and the 17 lowest energy structures were selected for further analysis. ProcheckNMR[30] was used to analyze the 17 lowest energy structures. Of residues 1–44, 81.2% and 18.8% (93% and 7% of residues 5–42) fell into the most favorable and additionally allowed regions, respectively.

NMR experiments on the AKAP–RIIα(1–44) complex. Ht31(493–515), an unlabeled, biotinylated peptide, was synthesized and purified to >95% homogeneity by PeptidoGenic Research and Co. (Livermore, CA). A 2 mM ^{15}N-labeled RIIα(1–44) NMR sample was titrated with increasing amounts of Ht31(493–515). A series of 2D ^{15}N-^{1}H HSQC experiments[23] were collected at points along the titration curve to monitor H^N chemical-shift changes that occurred in RIIα(1–44). Once a 1:1 complex was formed, no further chemical-shift changes were observed upon further addition of peptide.

Coordinates. The coordinates of the 17 structures have been deposited in the Protein Data Bank (accession code 1R2A).

Acknowledgments

This work was supported in part by grants from the NIH to M.G.N., Z.E.H., V.C., J.D.S. and P.A.J., the American Heart Association to M.G.N., the American Cancer Society to P.A.J. and the Cancer Research Coordinating Center to P.A.J.. We gratefully acknowledge A. Deese, D. Eliezer, M. Foster, I. Radhakrishnan, R. Kriwacki, Nicholas Skelton, J. Chung and J. Love for helpful discussions; and J. Adams, A. Newton, G. Ghosh and S. Taylor for their critical reading of this manuscript.

Correspondence should be addressed to P.A.J. *email: pajennin@ucsd.edu*

Received 19 August, 1998; accepted 19 November, 1998.

1. Faux, M.C. & Scott, J.D. *Trends Biochem. Sci.* **21**, 312–315 (1996).
2. Faux, M.C. & Scott, J.D. *Cell* **85**, 9–12 (1996).
3. Hubbard, M. & Cohen, P. *Trends Biochem. Sci.* **18**, 172–177 (1993).
4. Mochly-Rosen, D. *Science* **268**, 247–251 (1995).
5. Pawson, T. & Scott, J.D. *Science* **278**, 2075–2080 (1997).
6. Rubin, C.S. *Biochim. Biophys. Acta* **1224**, 467–479 (1994).
7. Dell'Acqua, M.L. & Scott, J.D. *J. Biol. Chem.* **272**, 12881–12884 (1997).
8. Scott, J.D. *Pharmacol. Ther.* **50**, 123–145 (1991).
9. Knighton D.R. *et al. Science* **253**, 407–414 (1991).
10. Su, Y. *et al. Science* **269**, 807–813 (1995).
11. Burton, K.A. *et al. Proc. Natl. Acad. Sci. USA* **94**, 11067–11072 (1997).
12. Newlon, M.G., Roy, M., Hausken, Z.E., Scott, J.D. & Jennings, P.A. *J. Biol. Chem* **272**, 23637–23644 (1997).
13. Nilges, M. *Proteins* **17**, 297–309 (1993).
14. Ikura, M., Kay, L.E., Tschudin, R. & Bax, A. *J. Magn. Reson.* **86**, 204–209 (1990).
15. Ikura, M. *et al. Science* **256**, 632–638 (1992).
16. Jeener, T., Meier, B.H., Bachman, P. & Ernst, R.R. *J. Chem. Phys.* **71**, 4546–4553 (1979).
17. Brunger, A.T. *X-PLOR Version 3.1:* a *system for X-ray crystallography and NMR* (Yale University Press, New Haven, Connecticutt; 1992).
18. Atkinson, R.A., Saudek, V., Huggins, J.P. & Pelton, J.T. *Biochemistry* **30**, 9387–9395 (1991).
19. Harris, N.L., Presnell, S.R. & Cohen, F.E. *J. Mol. Biol.* **236**, 1356–1368 (1994).
20. Crick, F.H.C. *Acta Crystallogr.* **6**, 689–697 (1953).
21. Li, Y. & Rubin, C.S. *J. Biol. Chem.* **270**, 1935–1944 (1995).
22. Leon, D.A., Herberg, F.W., Banky, P. & Taylor, S.S. *J. Biol. Chem.* **272**, 28431–28437 (1997).
23. Mori, S., Abeygunawardana, C., Johnson, A.O. & van Zijl, P.C.M. *J. Magn. Reson.* **108**, 94–98 (1995).
24. Wishart, D.S. & Sykes, B.D. *J. Biomol. NMR* **4**, 171–180 (1994).
25. Rustandi, R.R., Drohat, A.C., Baldisseri, D.M., Wilder, P.T. & Weber, D.J. *Biochemistry* **37**, 1951–1960 (1998).
26. Drohat, A.C. *et al. Biochemistry* **35**, 11577–11588 (1996).27. Potts, B.C. *et al. Nature Struct. Biol.* **2**, 790–796 (1995).
27. Potts, B.C. *et al. Nature Struct. Biol.* **2**, 790–796 (1997).
28. Faux, M.C. & Scott, J.D. *J. Biol Chem.* **272**, 17038–17044 (1995).
29. Vuister, G.W. & Bax, A. *J. Am. Chem. Soc.* **115**, 772–777 (1993).
30. Laskowski, R.A., Rullmann, A.C., MacArthur, M.W., Kaptein, R. & Thornton, M. *J. Biomol. NMR* **8**, 477–486 (1996).
31. Koradi, R., Billeter, M. & Wuthrich, K. *J. Mol. Graph.* **14**, 51–55 (1996).